Prokopiou, Sotiris A. and Byrne, Helen M. and Jeffrey, Mike R. and Robinson, Robert S. and Mann, George E. and Owen, Markus R. (2014) Mathematical analysis of a model for the growth of the bovine corpus luteum. Journal of Mathematical Biology, 69 (6). pp. 1515-1546. ISSN 0303-6812

Journal of Mathematical Biology manuscript No.
(will be inserted by the editor)

Mathematical analysis of a model for the growth of the bovine corpus luteum

Sotiris A. Prokopiou[1,2] · **Helen M. Byrne**[2,3] · **Mike R. Jeffrey**[4] · **Robert S. Robinson**[5] · **George E. Mann**[1] · **Markus R. Owen**[2]

Received: date / Accepted: date

Abstract The corpus luteum (CL) is an ovarian tissue that grows in the wound space created by follicular rupture. It produces the progesterone needed in the uterus to maintain pregnancy. Rapid growth of the CL and progesterone transport to the uterus require angiogenesis, the creation of new blood vessels from pre-existing ones, a process which is regulated by proteins that include fibroblast growth factor 2 (FGF2).

In this paper we develop a system of time-dependent ordinary differential equations to model CL growth. The dependent variables represent FGF2, endothelial cells (ECs), luteal cells, and stromal cells (like pericytes), by assuming that the CL volume is a continuum of the three cell types. We assume that if the CL volume exceeds that of the ovulated follicle, then growth is inhibited. This threshold volume partitions the system dynamics into two regimes, so that the model may be classified as a Filippov (piecewise smooth) system.

We show that normal CL growth requires an appropriate balance between the growth rates of luteal and stromal cells. We investigate how angiogenesis influences CL growth by considering how the system dynamics depend on the

S.A. Prokopiou, G.E. Mann
[1] School of Biosciences, University of Nottingham, Loughborough LE12 5RD, UK
E-mail: pmxsp@nottingham.ac.uk

M.R. Owen, H.M. Byrne, S.A. Prokopiou
[2] Centre for Mathematical Medicine and Biology, School of Mathematical Sciences, University of Nottingham, Nottingham NG7 2RD, UK

H.M. Byrne
[3] Oxford Centre for Collaborative Applied Mathematics, University of Oxford, 24-29 St Giles', Oxford OX1 3LB, UK and Department of Computer Science, University of Oxford, Oxford OX1 3QD, UK

M.R. Jeffrey
[4] Department of Engineering Mathematics, University of Bristol, Bristol BS8 1TR, UK

R.S. Robinson
[5] School of Veterinary Medicine, University of Nottingham, Loughborough LE12 5RD, UK

dimensionless EC proliferation rate, ρ_5. We find that weak (low ρ_5) or strong (high ρ_5) angiogenesis leads to 'pathological' CL growth, since the loss of CL constituents compromises progesterone production or delivery. However, for intermediate values of ρ_5, normal CL growth is predicted. The implications of these results for cow fertility are also discussed. For example, inadequate angiogenesis has been linked to infertility in dairy cows.

Keywords corpus luteum · angiogenesis · piecewise smooth systems · sliding bifurcations

1 Introduction

The corpus luteum (CL) is the tissue which develops from an ovarian follicle during the luteal phase of the oestrous or menstrual cycle (Fig 1(a)). It emerges from granulosa and theca cells which, after ovulation, differentiate into large and small steroidogenic luteal cells (LCs), respectively, via a process known as luteinisation which involves the transition of a pre-ovulated follicle into a highly vascular CL (Fig 1(b)). Following ovulation, the basement membrane that separates the granulosa and theca cells is broken down by matrix metalloproteinases and plasminogen activators. This enables endothelial cells (ECs) and pericytes (PCs) (located in the theca region before ovulation) to migrate into and vascularise the luteinising granulosa cells (Robinson et al., 2009).

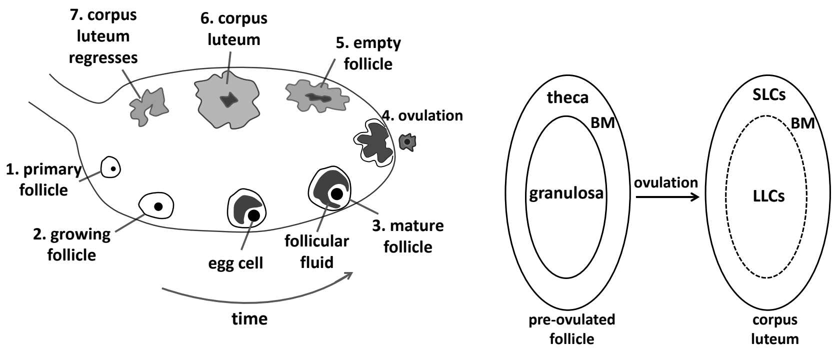

(a) (b)

Fig. 1 (a) Schematic diagram showing how the corpus luteum (CL) forms after ovulation in the ovary. At the end of the follicular phase of the menstrual cycle, the mature follicle ruptures (ovulation), the egg cell (oocyte) is released and the ruptured follicle undergoes a transformation into the CL. **Key:** follicular phase (1-3); ovulation (4); luteal phase (5-7); oestrous or menstrual cycle (1-7). (b) Schematic diagram showing the evolution of the CL (cross-section) structure after ovulation. **Key:** small luteal cells (SLCs); large luteal cells (LLCs); basement membrane (BM).

It is now well established that angiogenesis plays a key role in the growth and function of the CL (Reynolds and Redmer, 1996, 1999). Angiogenesis is the process by which new blood vessels develop from an existing vasculature (via the sprouting, proliferation and fusion of ECs). It occurs, in a controlled manner, during tissue repair, wound healing, placental development, and CL growth (Reynolds and Redmer, 1996). By contrast, uncontrolled angiogenesis underpins a variety of pathological conditions, such as diabetic retinopathy, arthritis, chronic inflammation and solid tumour growth.

The extensive vascularisation of the CL enables it to receive one of the highest blood flows per unit tissue mass and to supply the nutrients needed for its high metabolic rate (Reynolds and Redmer, 1996; Fraser and Lunn, 2001). The capillary network of the mature CL is so dense that most LCs are adjacent to one or more capillaries. This is perhaps not surprising, since in several mammals most (up to 85%) of the cells that proliferate during CL growth are ECs (Reynolds and Redmer, 1998). This enables the CL to grow at a rate (0.5 g to >5 g in 5 days (Robinson et al., 2007)) that is surpassed only by the fastest growing tumours. Such dramatic growth is essential for the CL to produce sufficient progesterone to support the developing embryo (Robinson et al., 2008).

The CL (mainly LCs (Juengel and Niswender, 1999)) secretes progesterone which regulates the length of the oestrous and menstrual cycles and is essential for maintenance of pregnancy. Inadequate progesterone is a major cause of early embryonic mortality (Juengel and Niswender, 1999). Therefore, impaired angiogenesis in the CL could cause poor embryonic development and infertility.

Angiogenesis in the CL is controlled by a plethora of angiogenic factors, including vascular endothelial growth factor (VEGF), fibroblast growth factor 2 (FGF2) and the platelet-derived growth factor (PDGF) family. These factors are thought to have complementary rather than redundant actions in luteal angiogenesis: the absence of any one signal is sufficient to cause marked alterations in endothelial network formation (Robinson et al., 2009). These studies clearly demonstrate that luteal endothelial cells are more sensitive to FGF2 inhibition than any other growth factor. Furthermore, there are dynamic changes in FGF2 concentration during the follicle-luteal transition (the point before and after ovulation) in the cow (see Fig 2(a)), while VEGFA concentrations remain constant (Robinson et al., 2009). Hence we focus on the role played by FGF2.

Even though the mechanisms responsible for the development, maintenance and regression of the CL have been extensively studied (for review, see (Hunter, 2003)), no mathematical models of this process have yet been developed. In the remainder of this section, we present data taken from (Robinson et al., 2007; Mann, 2009) to motivate the model that we develop.

Fig 2(a) shows how the FGF2 concentration in the CL changes in the 12 days that follow oestrous. The surge in FGF2 that occurs during ovulation (days 1-2) (Robinson et al., 2007) is followed by a rapid decrease until FGF2 levels settle to a steady value. The rapid change in FGF2 levels during the two days that proceed ovulation coincides with the initiation of angiogenesis in the early CL.

Fig 2(b) shows how the CL increases rapidly in size during the early and mid-luteal stages of the oestrous cycle (Mann, 2009). Fig 2(c)-(d) indicate how endothelial and pericyte numbers, respectively, in the CL change over time (Laird, 2010).

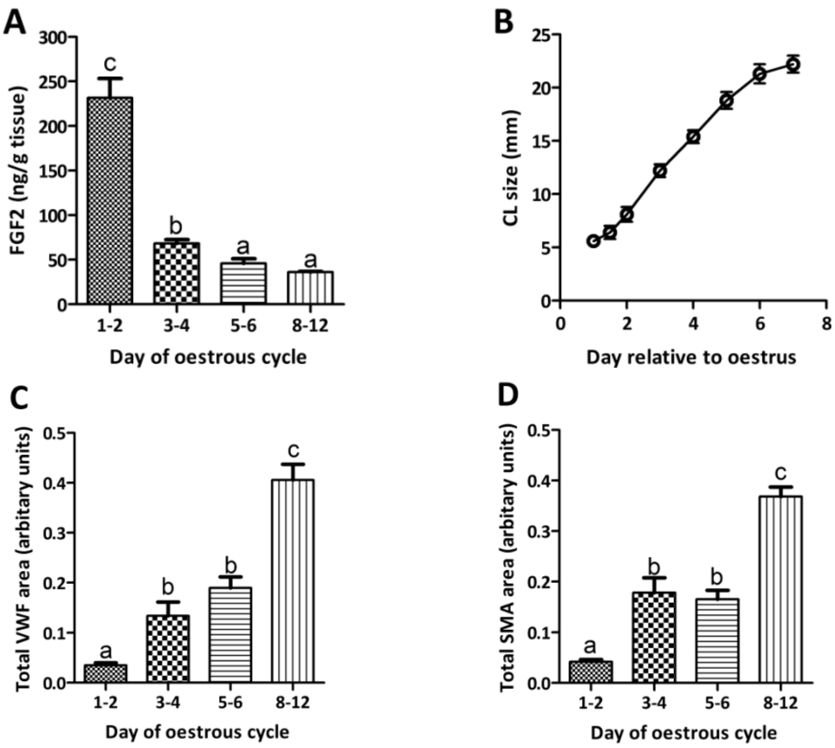

Fig. 2 Data on CL development following ovulation: (a) luteal FGF2 concentrations (Robinson et al., 2007), (b) CL size (diameter) (Mann, 2009), (c) total luteal endothelial cell area (Laird, 2010), and (d) total pericyte cell area during CL development (days 1 (ovulation) to 12 (mature CL)) (Laird, 2010). The data are mean + S.E.M.; significant differences between groups are indicated with a<b<c; P<0.05. The Von Willebrand Factor (VWF) and Smooth Muscle Actin (SMA) are endothelial and pericyte markers, respectively.

The main objective of this study is to develop a model that qualitatively reproduces existing experimental data on CL growth and development (Fig 2). This can then be used to explore the dependence of physiological and pathological behaviours on parameter values. This, in turn, will enable us to predict the potential effects of manipulating endothelial cells (angiogenesis) on the development of the CL, a crucial process in the establishment of pregnancy and fertility in dairy cows.

The remainder of the paper is organised as follows. We present the mathematical model in section 2, and in section 3 we identify regions of parameter space in which physically realistic steady states exist. We devote section 4 to describing how the evolution of the CL is affected by angiogenesis. The paper concludes in section 5 with a summary of our results and suggestions for future research directions.

2 Model overview

2.1 The mathematical model

In this section, we develop an ordinary differential equation (ODE) model for the time evolution of the CL in which the dependent variables represent the volumes of ECs, LCs, and all other, stromal cells (such as PCs). We denote by $F(t)$ the concentration of the growth factor, FGF2, and the volumes of the ECs, LCs and stromal cells by $E(t), L(t)$ and $R(t)$, respectively. We postulate that CL growth is due to cell division of ECs and stromal cells, and volumetric growth of LCs, and is regulated by the FGF2 contribution as explained below.

2.1.1 Growth factor FGF2, F(t)

Following (Robinson et al., 2007), we assume that ECs produce FGF2 at a constant rate, a_1, and LCs produce it at a rate which peaks during the two days that follow ovulation (see Fig 3). Following the disassembly of the theca vasculature after ovulation, extensive proliferation and migration of ECs helps to re-establish connections with other endothelial and luteal cells. This coincides

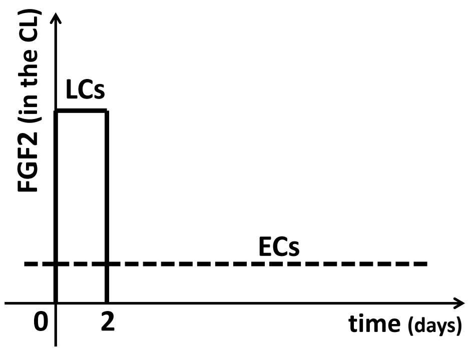

Fig. 3 Schematic illustration of FGF2 production during CL development. ECs produce FGF2 at constant rate (dotted line) throughout CL development, whereas LCs produce FGF2 for shorter time period (approximately 2 days) but at greater rate ($\sim$4 fold larger) (Schams et al., 2006; Robinson et al., 2007).

with a decrease in FGF2 concentration and the formation of new capillary beds (Robinson et al., 2009). Therefore, we hypothesize that when ECs attach to LCs, the rate of FGF2 production (by LCs) decreases. More specifically, we assume that the rate at which individual LCs produce FGF2 is a decreasing function of E/L:

$$\begin{pmatrix} rate\ at\ which\ individual \\ LCs\ produce\ FGF2 \end{pmatrix} = \frac{a_2}{R_{EL} + \frac{E}{L}}, \tag{1}$$

where the dimensionless parameter R_{EL} is the value of E/L at which FGF2 production (by LCs) is half-maximal. Combining the above processes (and noting that the net rate of FGF2 production by LCs is $a_2 L/(R_{EL} + E/L)$), we conclude that the evolution of FGF2 is given by:

$$\frac{dF}{dt} = a_1 E + \frac{a_2 L^2}{R_{EL} L + E} - d_F F, \tag{2}$$

where a_1, a_2, R_{EL} and d_F are positive constants, with d_F being the decay rate of FGF2.

The equations that describe the dynamics of the three cell types are of the following general form:

$$\frac{d}{dt}\begin{pmatrix} total\ volume \\ of\ cells \\ of\ type\ C \end{pmatrix} = \begin{pmatrix} rate\ of\ volume \\ increase\ due\ to \\ cell\ swelling\ or \\ proliferation \end{pmatrix} - \begin{pmatrix} rate\ of\ volume \\ loss\ due\ to \\ competition \\ for\ space \end{pmatrix}. \tag{3}$$

where $C = E, L, R$. We postulate that the CL is contained within an elastic membrane (Hunter, 2003). The ECs and stromal cells proliferate and increase in number, whereas LCs increase in volume, until eventually the CL volume ($V = E + L + R$) occupies the cavity ($\overline{V}$) left by the mature ovarian follicle after its rupture during ovulation. The surrounding membrane then becomes taut and exerts a restraining force on the cells which, if sufficiently large, leads to competition for space. We assume that this is the dominant mechanism for volume loss within the CL so that for each cell type the rate of cell death can be written as:

$$\begin{pmatrix} rate\ of \\ volume\ loss \\ of\ C \end{pmatrix} = kCVH(V - \overline{V}), \tag{4}$$

where the parameter k indicates how sensitive the cells' death rate is to competition for space. Implicit in equation (4) is the assumption that all cells are equally sensitive to competition for space. H is the Heaviside step function ($H(x) = 1$ if $x > 0,$ and $H(x) = 0$ otherwise).

2.1.2 Endothelial cells, E(t)

ECs react to free chemokines (e.g. FGF2). However, it is the presence of activated receptors on the cell surface that elicits a response from ECs. Responses such as proliferation result from the integration of the total number of activated receptors on their surfaces (Rieck et al., 1995; Laird et al., 2013). We assume that the number of FGF2 receptors on the endothelial cell membrane is finite and that they can be saturated. Accordingly, the EC proliferation rate is taken to be an increasing, saturating function of FGF2 and equations (3) and (4) give

$$\frac{dE}{dt} = k_E \frac{F}{F_h + F} E - kEVH(V - \overline{V}), \tag{5}$$

where the positive parameter k_E represents the maximal rate of EC proliferation, and F_h is the FGF2 concentration at which EC proliferation is half-maximal.

2.1.3 Luteal cells, L(t)

We account for the dependence of LC swelling on nutrient levels (Reynolds and Redmer, 1999) by assuming that the LC swelling rate is an increasing, saturating function of E:

$$\frac{dL}{dt} = k_L \frac{E}{E_{h_1} + E} L - kLVH(V - \overline{V}). \tag{6}$$

In equation (6) the positive parameter k_L is the maximal swelling rate of the LCs, and E_{h_1} is the volume of ECs at which the swelling rate is half-maximal.

2.1.4 Stromal cells, R(t)

We assume that the evolution of all stromal cells is similar to that of the ECs and the LCs, with

$$\frac{dR}{dt} = k_R \frac{E}{E_{h_2} + E} R - kRVH(V - \overline{V}). \tag{7}$$

In equation (7) the parameter k_R represents the maximal proliferation rate of the stromal cells, and E_{h_2} is the volume of ECs at which proliferation of the stromal cells is half-maximal.

In summary, our model consists of four ODEs (2),(5)-(7), which describe how the concentration of FGF2 and the volumes of endothelial, luteal and stromal cells change over time.

2.2 Parameter values

A list of the model parameters and their units are given in Table 1, and their values are estimated in Appendix A. The growth factor is measured in units ng/cm^3, the volumes of the different cell types in cm^3, and the time in days (d).

Before continuing with our investigation of equations (2),(5)-(7), it is appropriate to nondimensionalise and, in so doing, to reduce the number of system parameters.

Table 1 Dimensional parameter values used in equations (2),(5)-(7).

Parameter	Value	Unit	Reference
a_1	136	$ng.(cm^3)^{-2}.d^{-1}$	estimated
a_2	5.1	$ng.(cm^3)^{-2}.d^{-1}$	estimated
k	0.12	$(cm^3)^{-1}.d^{-1}$	estimated
d_F	3	d^{-1}	(Beenken and Mohammadi, 2009)
k_E	1	d^{-1}	(Lincoln et al., 1982)
k_L	1	d^{-1}	(Lincoln et al., 1982)
k_R	1	d^{-1}	(Lincoln et al., 1982)
F_h	50	$ng.(cm^3)^{-1}$	estimated
E_{h_1}	1.1	cm^3	estimated
E_{h_2}	1.1	cm^3	estimated
$\overline{V}$	8.2	cm^3	estimated
R_{EL}	0.2	-	estimated

2.3 Nondimensional model

We nondimensionalise equations (2),(5)-(7) by choosing $F(t)=F_h\hat{F}(\hat{t})$, $E(t)=\overline{V}\hat{E}(\hat{t})$, $L(t)=\overline{V}\hat{L}(\hat{t})$, $R(t)=\overline{V}\hat{R}(\hat{t})$ and $t=\frac{\hat{t}}{k\overline{V}}$, where, $\hat{F}$, $\hat{E}$, $\hat{L}$, $\hat{R}$ are the dimensionless dependent variables and $\hat{t}$ is the dimensionless time. By substituting for F, E, L, R and t, in (2),(5)-(7) we obtain the following dimensionless equations (hats have been dropped for notational convenience):

$$\frac{dF}{dt} = \rho_1 E + \rho_2 \frac{L^2}{\rho_3 L + E} - \rho_4 F, \tag{8}$$

$$\frac{dE}{dt} = \rho_5 \frac{F}{1+F} E - EVH(V-1), \tag{9}$$

$$\frac{dL}{dt} = \rho_6 \frac{E}{\rho_7 + E} L - LVH(V-1), \tag{10}$$

$$\frac{dR}{dt} = \rho_8 \frac{E}{\rho_9 + E} R - RVH(V-1), \tag{11}$$

where $V = E + L + R$, and the dimensionless parameters are given by:

$$\begin{aligned} &\rho_1 = \tfrac{a_1}{kF_h}, \quad \rho_2 = \tfrac{a_2}{kF_h\overline{V}}, \quad \rho_3 = R_{EL}, \quad \rho_4 = \tfrac{d_F}{k\overline{V}}, \quad \rho_5 = \tfrac{k_E}{k\overline{V}}, \\ &\rho_6 = \tfrac{k_L}{k\overline{V}}, \quad \rho_7 = \tfrac{E_{h_1}}{\overline{V}}, \quad \rho_8 = \tfrac{k_R}{k\overline{V}}, \text{ and } \rho_9 = \tfrac{E_{h_2}}{\overline{V}}. \end{aligned} \tag{12}$$

The dimensionless parameter values used to generate the numerical simulations in section 2.5 were estimated by using equation (12) and the dimensional values stated in Table 1:

$$\begin{aligned} &\rho_1 = 23, \quad \rho_2 = 0.1, \quad \rho_3 = 0.19, \quad \rho_4 = 3, \quad \rho_5 = 1, \\ &\rho_6 = 1, \quad \rho_7 = 0.13, \quad \rho_8 = 1, \quad \rho_9 = 0.13. \end{aligned} \tag{13}$$

2.4 Initial conditions

In the mid-cycle bovine CL, small and large steroidogenic (luteal) cells constitute approximately 68% of the CL volume, the ECs approximately 13%, and therefore, the other cell types account for the remaining 19% of the total volume (Wiltbank, 1994). *In vivo*, it can be difficult accurately to define the boundary of the CL immediately post ovulation as the CL can have a similar ultrasonographic appearance to the rest of the ovarian stroma. However, within 24 hrs the boundaries of the CL can be accurately determined and based on this we have estimated the diameter of the CL to be 8 mm on day 1, resulting in $V(t = 1) \simeq \frac{4}{3}\pi R^3 = 0.27$ cm^3. We close equations (8)-(11) by imposing the following initial conditions:

$$F(0) = 4.0, \quad E(0) = 0.04, \quad L(0) = 0.18, \quad R(0) = 0.05, \tag{14}$$

with $F(0)$ estimated from Fig 2(a) and the value of F_h (as stated in Table 1) since $F(t){=}F_h\hat{F}(\hat{t})$.

2.5 Typical numerical results

The Heaviside step function that appears in equations (9)-(11) introduces a discontinuity into the right-hand sides of equations (9)-(11) at $V = 1$ (the *'discontinuity boundary'* (Bernardo et al., 2008)), making the system *piecewise-smooth* (PWS) (Bernardo et al., 2008; Filippov, 1982). We solve the system using Piiroinen's method (Piiroinen and Kuznetsov, 2008), which applies instantaneous resets at the discontinuity (events), by accurately locating the times at which $V = 1$.

In Fig 4 we plot the evolution of F, E, L, R and V for a typical simulation. These results are in good qualitative agreement with the *in vivo* data presented in Fig 2. Regarding the FGF2 profile, it should be noted that although the data (Fig 2) display only a decrease of FGF2, in the simulation (Fig 4(a)) there is a strong decrease of its level, which reaches a minimum, then increases and reaches a plateau. This is of course not an exact representation of the reality, however, from a biological point of view, the important observation is the transient, greatly (∼4 fold) increased levels of FGF2 at ovulation ($t = 0$) followed by a decrease which then plateau is reached afterwards.

The loss terms in equations (9)-(11) switch on at time t^*, when V increases above the threshold $V = 1$. In biological terms, t^* delineates the shift from the early-mid to the mid-late luteal (vascularised) stage. For $t < t^*$ and $V < 1$ the cells do not experience any growth constraints (Fig 4(b)). In contrast, for $t > t^*$ total CL volume remains fixed ($V = 1$), but relative constituents of difference cell types change (Fig 4(b)).

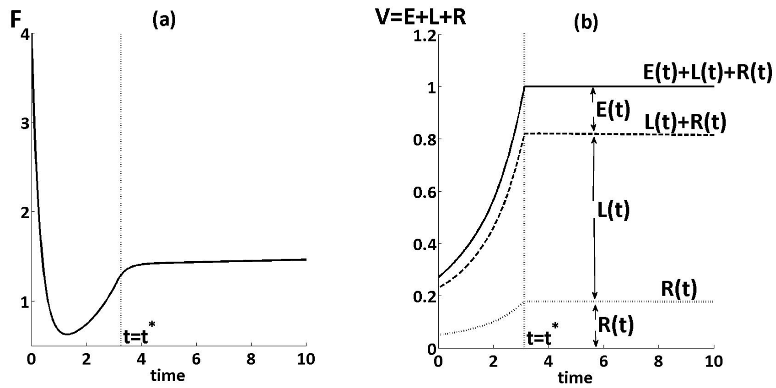

Fig. 4 Profiles of (a) the FGF2 concentration, $F(t)$, and (b) the CL volume, $V(t) = E(t) + L(t) + R(t)$. The numerical results were obtained by solving the dimensionless model defined by equations (8)-(11) and subject to the initial conditions (14). The parameter values are specified in equation (13). Note that $t = t^*$ is the first time point where $V = 1$, which implies the activation of the volume loss terms for each cell type (E, L, R) in equations (9)-(11).

2.6 A simplified model

Equations (8)-(11) define a fourth-order system of ODEs, whose trajectories are difficult to visualise in phase space. Before analysing the full model, we consider the simpler case for which $L = R = 0$, and $V \approx E$ so that equations (8)-(11) reduce, at leading order, to the following pair of ODEs:

$$\left.\begin{array}{ll} FGF2: & \frac{dF}{dt} = \rho_1 E - \rho_4 F, \\ CL\ volume: & \frac{dE}{dt} = \rho_5 \frac{F}{1+F} E - E^2 H(E-1). \end{array}\right\} \quad (15)$$

The behaviour of equations (15) depends on whether $E < 1$ or $E > 1$, the two types of behaviour being separated by the boundary $E = 1$. Analysis of this simplified model guides our subsequent study of the full model.

2.6.1 Phase plane analysis and steady states

Insight into the dynamics of this model can be obtained by identifying its nullclines. Fig 5 shows that the nullcline $\frac{dF}{dt} = 0$ is a line N_1 on which $E = \frac{\rho_4}{\rho_1} F$. The nullclines on which $\frac{dE}{dt} = 0$ include the curve N_2 on which $E = \rho_5 \frac{F}{1+F}$ (when $E > 1$), together with the coordinate axes $F = 0$ and $E = 0$ (when $E < 1$). Fig 5 shows how the system dynamics change as ρ_5 (the maximum EC proliferation rate) varies.

Interestingly, in Fig 5(a) the discontinuity boundary $E = 1$ is shown to be attractive from both sides ($E < 1$ or $E > 1$) regardless of the value of F, while in Figs 5(b)-(c) this occurs only for $F < F_2 = \frac{1}{\rho_5 - 1}$ (where $F2$ is the value of FGF2 at the intersection of nullcline N_2 with the discontinuity boundary). That is, the trajectories evolve onto $E = 1$, a behaviour called *sliding* (Bernardo et al., 2008) which is defined in section 2.7.

Equations (15) admit two steady states (where $\frac{dE}{dt} = \frac{dF}{dt} = 0$): we denote by B_0 the trivial solution $(F, E) = (0, 0)$ and by B_1 the nontrivial solution $(F, E) = (\Gamma, \frac{\rho_4}{\rho_1}\Gamma)$, where $\Gamma = \frac{\rho_1 \rho_5}{\rho_4} - 1$. The steady state B_1 exists where $E > 1$ or, equivalently,

$$\rho_5 > \rho_5^* := \frac{\rho_4}{\rho_1} + 1. \tag{16}$$

Figs 5(a)-(b) show that when $\rho_5 < \rho_5^*$ sliding states are attracted towards a point B_{1s} at which $(F, E) = (\frac{\rho_1}{\rho_4}, 1)$, and the competing flows from $E > 1$ and $E < 1$ are equal and opposite. This point is called a *'pseudo steady state'* (or pseudo-equilibrium (Bernardo et al., 2008)). As ρ_5 increases through $\rho_5 = \rho_5^*$, the steady B_{1s} approaches the point where N_1 crosses $E = 1$ at $(\frac{1}{\rho_5 - 1}, 1)$, then B_{1s} vanishes, and B_1 appears at the same point and detaches from $E = 1$ into the region $E > 1$ (Fig 5(c)). This is an example of a *boundary equilibrium bifurcation* (see below and (Colombo, 2009; Bernardo et al., 2008)).

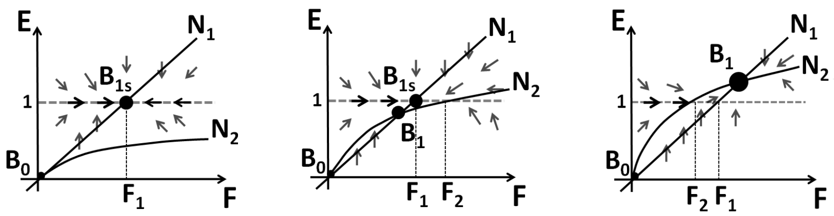

(a) $\rho_5 \ll \rho_5^* = 1 + \frac{\rho_4}{\rho_1}$ (b) $\rho_5 < \rho_5^*$ (c) $\rho_5 > \rho_5^*$

Fig. 5 Phase plane diagrams for equations (15) showing how the system dynamics change as ρ_5 varies. *Sliding* occurs along the discontinuity boundary $E = 1$ towards the *pseudo-*steady state, B_{1s}. **Key:** N_1 and N_2 are nullclines on which $E = \frac{\rho_4}{\rho_1} F$ and $E = \rho_5 \frac{F}{1+F}$, respectively. The points $F_1 = \frac{\rho_1}{\rho_4}$ and $F_2 = \frac{1}{\rho_5 - 1}$ lie at the intersections of N_1 and N_2 and the discontinuity boundary, $E = 1$. Note that B_1 does not exist for $\rho_5 < \rho_5^*$, and N_2 exists for $E > 1$.

2.6.2 Conclusions from the simplified model

When $\rho_5 > \rho_5^*$ equations (15) evolve to a steady state B_1 for which $E > 1$ (Fig 5(c)), while for $\rho_5 < \rho_5^*$ the system evolves to a *'pseudo steady state'* B_{1s} that lies on the discontinuity boundary $E = 1$ (Figs 5(a)-(b)).

Physically speaking, high ρ_5 (high EC proliferation) implies a large CL, bigger than the wound space formed after ovulation. Smaller EC proliferation implies a minimum size of the CL ($V = 1$). Similar behaviour is expected in the full model, the main difference being that the composition of the CL must also be determined. In the next paragraph we return to the full model and in section 3 we identify its steady state solutions.

2.7 The full model as a Filippov system

We now express equations (8)-(11) in the form that is typically used for piecewise-smooth (or Filippov (Filippov, 1982)) systems, namely

$$\frac{d\underline{x}}{dt} = \begin{cases} \underline{f}^+(\underline{x}) \ , \ \Theta(\underline{x}) > 0, \\ \underline{f}^-(\underline{x}) \ , \ \Theta(\underline{x}) < 0, \end{cases} \tag{17}$$

by setting $\underline{x} = (F, E, L, R) \in \mathbb{R}^4$ and defining

$$\underline{f}^+ := \underline{f}^- - (E + L + R) \begin{pmatrix} 0 \\ E \\ L \\ R \end{pmatrix}, \tag{18}$$

and

$$\underline{f}^- := \begin{pmatrix} \rho_1 E + \rho_2 \frac{L^2}{\rho_3 L + E} - \rho_4 F \\ \rho_5 \frac{F}{1+F} E \\ \rho_6 \frac{E}{\rho_7 + E} L \\ \rho_8 \frac{E}{\rho_9 + E} R \end{pmatrix}. \tag{19}$$

The region of state space, $D \subset \mathbb{R}^4$, in which equations (17)-(19) govern the system dynamics, can be partitioned into two subregions, G^+ and G^- (see Fig 6), where

$$G^+ = \{\underline{x} \in \mathbb{R}^4, \ \Theta(\underline{x}) > 0\} \quad \text{and} \quad G^- = \{\underline{x} \in \mathbb{R}^4, \ \Theta(\underline{x}) < 0\}, \tag{20}$$

and $\Theta(\underline{x}) = E + L + R - 1 = V - 1$. The discontinuity boundary is a smooth hypersurface, Σ, given by:

$$\Sigma = \{\underline{x} \in \mathbb{R}^4, \ \Theta(\underline{x}) = 0\}. \tag{21}$$

Σ separates trajectories on which CL growth is constrained (G^+) from regions in which the CL grows without restriction (G^-). Thus the model is a nonlinear system with an 'on-off' feedback controller (the 'on-off' feedback being due to the Heaviside step function) specified by the CL volume, V.

Let the subscript $\underline{x}$ denote differentiation with respect to $\underline{x} = (F, E, L, R)$, so that $\Theta_{\underline{x}}(\underline{x}) = (0, 1, 1, 1)$ is the normal vector to Σ, and let $\langle ., . \rangle$ denote the scalar product. Then consider the quantity

$$\langle \Theta_{\underline{x}}(\underline{x}), \underline{f}^-(\underline{x}) \rangle = E\Omega, \tag{22}$$

where

$$\Omega \ := \ \frac{\rho_5 F}{1+F} + \frac{\rho_6 L}{\rho_7 + E} + \frac{\rho_8 R}{\rho_9 + E}. \tag{23}$$

The scalar product is strictly non-negative since F, E, L, R are positive or zero (to be biologically realistic) and $\rho_i > 0$ for all i. This means that $\underline{f}^-$ always points towards $\Theta = 0$, so the discontinuity boundary $V = 1$ is attractive with respect to G^- ('attractive from below', as was the case for the 2D model in section 2.6).

Depending on whether $\underline{f}^+$ points towards or away from the discontinuity boundary, two kinds of motion are now possible when $\Theta = 0$. These are known as *crossing* and *sliding*, and occur when the quantity

$$\langle \Theta_{\underline{x}}(\underline{x}), \underline{f}^+(\underline{x}) \rangle \ = \ E\Omega - 1 \tag{24}$$

is positive and negative respectively. If $\langle \Theta_{\underline{x}}(\underline{x}), \underline{f}^+(\underline{x}) \rangle > 0$, then the vector field $\underline{f}^+$ points away from Σ, implying that trajectories evolve from G^- to G^+ by crossing Σ. Otherwise, $\underline{f}^+$ points towards Σ, so that the discontinuity boundary attracts trajectories from both G^+ and G^-, and solutions must slide along Σ. When sliding occurs, the CL volume remains fixed at the threshold value, $V = 1$. We denote the sliding region by $\hat{\Sigma}$ (see Fig 6), where

$$\hat{\Sigma} = \Big\{ \underline{x} \in \Sigma, \quad 0 \leqslant E\Omega \leqslant 1 \Big\}. \tag{25}$$

Its boundaries are given by

$$\partial\Sigma^+ := \Big\{ \underline{x} \in \Sigma : E\Omega = 1 \Big\} \quad \text{and} \quad \partial\Sigma^- := \Big\{ \underline{x} \in \Sigma : E\Omega = 0 \Big\}. \tag{26}$$

On these surfaces the flow is tangent to the discontinuity boundary: at $\partial\Sigma^+$ the condition $E\Omega = 1$ means $\underline{f}^+(\underline{x})$ is tangent to Σ, while at $\partial\Sigma^-$ the condition $E\Omega = 0$ means $\underline{f}^-(\underline{x})$ is tangent to Σ.

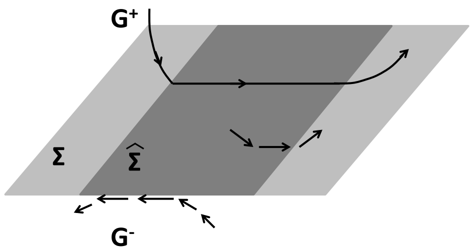

Fig. 6 The phase space topology of a Filippov system with discontinuous vector fields. The discontinuity boundary, Σ, separates the phase space into two regions (G^+, G^-), and each region is governed by a different smooth vector field ($\underline{f}^+(\underline{x}), \underline{f}^-(\underline{x})$). Solutions of equations (17)-(19) that are attracted to the sliding region ($\hat{\Sigma}$; dark grey) follow a constrained motion on Σ.

2.7.1 Regular and sliding solutions

Using the above decomposition, we construct solutions of system (17) by considering separately *regular* solutions in $G^{+/-}$ and *sliding* solutions on Σ. Following Filippov (Kuznetsov et al., 2003) we introduce $\underline{g}(\underline{x})$, a convex combination of the two vectors $\underline{f}^{\pm}(\underline{x})$,

$$\underline{g}(\underline{x}) = \lambda(\underline{x})\underline{f}^+(\underline{x}) + (1 - \lambda(\underline{x}))\underline{f}^-(\underline{x}), \quad 0 \leqslant \lambda \leqslant 1, \tag{27}$$

with each nonsingular point in the sliding region, i.e. $\underline{x} \in \hat{\Sigma}$ such that $\langle \Theta_{\underline{x}}(\underline{x}), \underline{f}^-(\underline{x}) - \underline{f}^+(\underline{x}) \rangle \neq 0$. The function λ is defined as

$$\lambda(\underline{x}) = \frac{\langle \Theta_{\underline{x}}(\underline{x}), \underline{f}^-(\underline{x}) \rangle}{\langle \Theta_{\underline{x}}(\underline{x}), \underline{f}^-(\underline{x}) - \underline{f}^+(\underline{x}) \rangle} = E\Omega, \tag{28}$$

so that $\underline{g}(\underline{x})$ is everywhere tangent to $\hat{\Sigma}$. We then add the equation

$$\dot{\underline{x}} = \underline{g}(\underline{x}), \quad \underline{x} \in \hat{\Sigma}, \tag{29}$$

to the system (17), thus extending its definition to include the discontinuity boundary. Solutions of (29) are called *'sliding solutions'*, and $\underline{g}(\underline{x})$ is called the '*sliding vector field*' (Bernardo et al., 2008), given by

$$\underline{g}(\underline{x}) = \begin{pmatrix} \rho_1 E + \rho_2 \frac{L^2}{\rho_3 L + E} - \rho_4 F \\ \rho_5 \frac{F}{1+F} E - E^2 \Omega \\ \rho_6 \frac{E}{\rho_7 + E} L - EL\Omega \\ \rho_8 \frac{E}{\rho_9 + E} R - ER\Omega \end{pmatrix}. \tag{30}$$

Solutions are then defined in the following way:

Definition 5.1. A *regular orbit* is a smooth trajectory of the system (17), which does not cross the discontinuity boundary $\Theta = 0$. A *sliding orbit* is a smooth trajectory of (29), that lies on the discontinuity boundary. An *orbit* will generally refer to a continuous curve $\underline{x}(t)$ that is a concatenation of regular and sliding orbits.

The *crossing set* $\underline{x} \in \Sigma\backslash\hat{\Sigma}$ is defined as the set of all points $\underline{x} \in \Sigma$ for which the two vectors, $\underline{f}^{\pm}(\underline{x})$, have nontrivial transverse components to Σ. At these points a regular orbit of (17) reaching $\underline{x}$ from G^- (region below Σ) concatenates with a regular orbit entering G^+ (region above Σ) from $\underline{x}$. At points in the sliding set, $\underline{x} \in \hat{\Sigma}$, a regular orbit of (17) reaching $\underline{x}$ from each of G^+ and G^- concatenates with a sliding orbit inside $\hat{\Sigma}$ passing through $\underline{x}$. All other points on Σ belong to the sliding boundaries $\partial\Sigma^{\pm}$, and can be treated as either sliding or crossing points without ambiguity.

It is a standard feature of piecewise-smooth systems that, although solutions evolve uniquely as time advances, sliding solutions do not have unique histories.

Steady states are defined as points at which $\underline{f}^+(\underline{x}) = 0$ or $\underline{f}^-(\underline{x}) = 0$, and pseudo steady states as points at which $\underline{g}(\underline{x}) = 0$. These are only admissible solutions if they lie in the appropriate regions, namely G^+, G^-, and $\hat{\Sigma}$, respectively. An explanation of the admissibility conditions is presented in Appendix B.

3 Analytical results

Henceforth, steady states in vector field $\underline{f}^{\pm}(\underline{x})$ will be indicated by a superscript $\pm$, and those in the sliding vector field $\underline{g}(\underline{x})$ by a superscript s.

The steady states in the regions G^+ and G^-, and in the sliding region $\hat{\Sigma}$, satisfy the relations in Table 2.

Table 2 Steady state expressions and admissibility conditions for steady states in regions $G^{+/-}$ and $\hat{\Sigma}$.

region	steady state expression	admissibility condition
G^+	$\underline{f}^+(\underline{x}) = \underline{0}$	$V \geqslant 1$
G^-	$\underline{f}^-(\underline{x}) = \underline{0}$	$V \leqslant 1$
$\hat{\Sigma}$	$\underline{g}(\underline{x}) = \underline{0}$	$0 \leqslant E\Omega \leqslant 1$

In addition to the admissibility condition (see Definitions 5.2 and 5.4 in Appendix B), each model variable F, E, L, R, must be positive for the steady state to be physically realistic. In the following, we list all steady states that satisfy these conditions and in Appendix B we translate criteria for solutions to be admissible and physically realistic into constraints on the parameters ρ_i $(i = 1, ..., 9)$.

3.1 Steady states in G^+

There are four steady states $A_i^+ = (F_i, E_i, L_i, R_i)$, $i = 1, ..., 4$ in G^+,

$$\begin{aligned} A_1^+ &:= E_1\left(\phi(E_1), 1, \psi(E_1), \nu(E_1) - \psi(E_1) - 1\right), && (31)\\ A_2^+ &:= E_2\left(\rho_1/\rho_4, 1, 0, \eta(E_2) - 1\right), && (32)\\ A_3^+ &:= E_3\left(\phi(E_3), 1, \nu(E_3) - 1, 0\right), && (33)\\ A_4^+ &:= E_4\left(\rho_1/\rho_4, 1, 0, 0\right), && (34) \end{aligned}$$

where,

$$\phi(E) := \frac{\rho_6}{\rho_5\rho_7 + (\rho_5 - \rho_6)E}, \quad \nu(E) := \frac{\rho_6}{\rho_7 + E}, \quad \eta(E) := \frac{\rho_8}{\rho_9 + E}, \qquad (35)$$

$$\begin{aligned} \psi(E) &:= \frac{\rho_3\omega(E) + \sqrt{(\rho_3\omega(E))^2 + 4\rho_2\omega(E)}}{2\rho_2}, && (36)\\ \omega(E) &:= \rho_4\phi(E) - \rho_1, && (37) \end{aligned}$$

$$E_1 := \frac{\rho_6\rho_9 - \rho_7\rho_8}{\rho_8 - \rho_6}, \quad E_2 = \frac{\rho_4\rho_8 - \rho_1\rho_5\rho_9}{\rho_1(\rho_5 - \rho_8)}, \quad E_4 = \rho_5 - \frac{\rho_4}{\rho_1}. \qquad (38)$$

and E_3 solves the following cubic polynomial

$$\rho_2(\nu(E_3) - 1)^2 - \rho_3\omega(E_3)(\nu(E_3) - 1) - \omega(E_3) = 0. \qquad (39)$$

For a physically realistic and admissible solution, we require all components of A_i^+, $(i = 1, ..., 4)$ to be positive and the corresponding volume to be such that $V = E + L + R > 1$. These conditions lead to constraints on the parameters ρ_i given in Appendix B (see equations (57)-(66)). Note also that the steady states in the vector field $\underline{f}^+(\underline{x})$ are vascular, that is, they have $E > 0$. If $\underline{f}^+(\underline{x}) = \underline{0}$ and $E = 0$ then the only possible steady state has $\underline{x} = \underline{0}$, and $V = 0$. This is not an admissible steady state in G^+ ($V > 1$ for an admissible solution).

3.2 Steady states in $\hat{\Sigma}$

For each steady state solution (31)-(34) in G^+, there is a similar steady state $A_i^s = (F_i, E_i, L_i, R_i)$, $i = 1, ..., 4$ in $\hat{\Sigma}$,

$$A_1^s := E_1 \left(\phi(E_1), 1, \psi(E_1), \frac{1}{E_1} - \psi(E_1) - 1 \right), \tag{40}$$

$$A_2^s := E_2 \left(\frac{\rho_1}{\rho_4}, 1, 0, \frac{1}{E_2} - 1 \right), \tag{41}$$

$$A_3^s := E_3^s \left(\phi(E_3^s), 1, \frac{1}{E_3^s} - 1, 0 \right), \tag{42}$$

$$A_4^s := \left(\frac{\rho_1}{\rho_4}, 1, 0, 0 \right). \tag{43}$$

The functions ϕ and ψ are given by (35) and (36), and the constants E_1, E_2 by (38), while E_3^s solves the following cubic polynomial

$$\rho_2(E_3^s - 1)^2 - \rho_3 E_3^s \omega(E_3^s)(1 - E_3^s) - E_3^s \omega(E_3^s) = 0. \tag{44}$$

The admissibility conditions associated with the steady states in G^+ and $\hat{\Sigma}$ are presented in Appendix B (see equations (67)-(72)).

3.3 Steady states in G^-

Any solution of the form

$$A^- = \left(\frac{\rho_2}{\rho_3 \rho_4} u, 0, u, v \right), \tag{45}$$

satisfies the steady state expression in Table 2, and is physical and admissible over the range $0 \leqslant v \leqslant 1 - u$ and $0 \leqslant u < 1 - v$. By varying u and v over these ranges, A^- forms a set of steady states lying in a planar surface Π^-, given by

$$\Pi^- = \left\{ (F, E, L, R) \in G^- : \ F = \frac{\rho_2}{\rho_3 \rho_4} L, \ E = 0 \right\}. \tag{46}$$

A stability analysis of the plane Π^- (see Appendix C) reveals that it is not a global attractor.

3.4 The 5th steady state in $\hat{\Sigma}$

Where the plane Π^- (shown in Fig 7) intersects the discontinuity boundary $V = 1$, it forms a family of steady states of the sliding vector field that does not coincide with any of the steady states A_n^s above. Thus any state of the form

$$A_5^s = \left(\frac{\rho_2}{\rho_3 \rho_4} u, 0, u, 1 - u \right), \tag{47}$$

satisfies the steady state expression in Table 2, and is physical and admissible provided that $0 \leqslant u \leqslant 1$. Note that $E = 0$ implies $E\Omega = 0$, therefore from (26) we have $A_5^s \in \partial\Sigma^-$. Thus the states A_5^s (shown in Fig 7) do not lie on the interior of the region $\hat{\Sigma}$, but on its boundary $\partial\Sigma^-$. Since u is a variable, the set of states A_5^s belongs to a line given by

$$\Pi^s = \left\{ (F, E, L, R) \in \partial\Sigma^- : \ F = \frac{\rho_2}{\rho_3\rho_4} L, \ E = 0, \ V = 1 \right\}. \qquad (48)$$

We remark that there are two limiting cases of equation (47) which we denote by $A_{5a}^s = (0, 0, 0, 1)$ and $A_{5b}^s = (\frac{\rho_2}{\rho_3\rho_4}, 0, 1, 0)$, respectively.

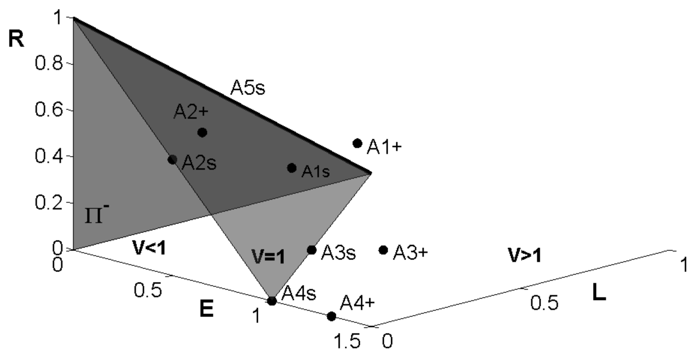

Fig. 7 Schematic showing the three-dimensional projections of four-dimensional phase portraits. Steady states are presented for the two different regions of phase space ($V > 1$ and $V < 1$) and the discontinuity boundary, $V = 1$. The steady state A_5^s defines a 1-D manifold in the discontinuity boundary.

4 Bifurcation analysis

Although numerical simulations for particular values of the system parameters provide some insight into the system's dynamics, a more complete understanding relies on determining parameter values at which the qualitative behaviour of these solutions change, i.e. *bifurcations.* (For a discussion of how to define bifurcations in piecewise-smooth systems, see (Bernardo et al., 2008)). An important characteristic of any bifurcation is its *codimension* - this is the number of parameters that need to be varied in order for the bifurcation to occur. In this section only codimension one bifurcations are considered.

4.1 Steady state bifurcations at the discontinuity boundary

The admissibility conditions for A_i^+ and A_i^s are summarised in Table 3 (for details see Appendix B) which shows that the parameter ranges for existence of any two steady states labelled by the same i are mutually exclusive, except at boundaries where A_i^+ and A_i^s coalesce on the switching boundary. For example, A_3^+ $(R = 0; V > 1)$ and A_3^s $(R = 0; V = 1)$ coincide when $\nu(E_3) = 1/E_3$ (compare (33) to (42)) or, equivalently, when $E_3 = E_3^s = \frac{\rho_7}{1-\rho_6}$.

Table 3 Admissibility conditions for steady states

steady state	parameter grouping	in G^+	in $\hat{\Sigma}$	boundary
$i = 1$	$\frac{\rho_6\rho_9-\rho_7\rho_8}{\rho_9-\rho_7}$	$\geqslant 1$	$\leqslant 1$	$\rho_6 = \rho_6^* := 1 - \frac{\rho_7}{\rho_9}(1-\rho_8)$
$i = 2$	$\frac{\rho_4\rho_8-\rho_1\rho_5\rho_9}{\rho_4-\rho_1\rho_9}$	$\geqslant 1$	$\leqslant 1$	$\rho_5 = \rho_5^{2*} := 1 - \frac{\rho_4}{\rho_1\rho_9}(1-\rho_8)$
$i = 3$	$\frac{\rho_6 E_3}{\rho_7+E_3}$	$\geqslant 1$	$\leqslant 1$	$\rho_5 = \rho_5^{3*} := \left(1 + \frac{\rho_4(\rho_6-1)(\rho_7+\rho_3\mu)}{\rho_2\mu^2+\rho_1\rho_7(\rho_7+\rho_3\mu)}\right)$, $\mu = \rho_6 - (1+\rho_7)$
$i = 4$	$\frac{\rho_1\rho_5}{\rho_1+\rho_4}$	$\geqslant 1$	$\leqslant 1$	$\rho_5 = \rho_5^{4*} := 1 + \frac{\rho_4}{\rho_1}$

The composition and volume (V) of the CL vary as ρ_5, the maximum rate of EC proliferation, changes for steady states $i = 2, 3, 4$ in Table 3. The bounds in this table are examples of a particular class of *discontinuity-induced bifurcations* known as *boundary equilibrium bifurcations* (Colombo, 2009; Bernardo et al., 2008). As ρ_5 passes through a bifurcation value ρ_5^{j*} (where $j = 2$, 3, or 4), a steady state A_j^+ hits the discontinuity boundary and disappears, while a sliding steady state A_j^s is created on the discontinuity boundary (or vice versa). Since one steady state always persists through the bifurcation, this scenario is classified as *persistence*. As an example, the persistence of A_4^s $(L = R = 0; V = 1)$ to A_4^+ $(L = R = 0; V > 1)$ as ρ_5 increases through ρ_5^{4*} is illustrated in Fig 8.

4.2 Perturbation of ρ_5: the maximum EC proliferation rate

The parameter ρ_5 represents the maximum rate of EC proliferation (see equation (9)), and by varying it we can assess how CL growth (e.g. volume, V), and its cellular composition (e.g. ECs, LCs, and stromal cells) are affected by the amount of angiogenesis that takes place.

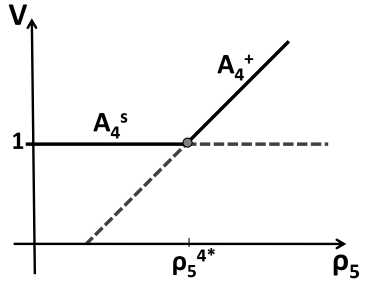

Fig. 8 Schematic bifurcation diagram for CL volume, $V = E + L + R$, as ρ_5 varies showing the *persistence* that is associated with a boundary equilibrium bifurcation. For $\rho_5 < \rho_5^{4*}$, A_4^+ is a virtual steady state, and A_4^s is an admissible pseudo steady state. For $\rho_5 > \rho_5^{4*}$, A_4^+ is admissible and A_4^s is virtual. Thus, there is one admissible (pseudo-) steady state on either side of the bifurcation point. **Key:** solid lines represent admissible solutions; dashed lines represent virtual ones (for details, see Appendix B).

In Table 1 we fix $k_E = k_L = k_R$ (so that the maximum growth rate for all cell types is identical) and $E_{h1} = E_{h2}$ (so that LCs and stromal cells have the same demand for nutrients and vasculature), and hence $\rho_6 = \rho_8$ and $\rho_7 = \rho_9$. These parameter values lead to singular value for the steady states $A_1^{+,s}$, since both the numerator and denominator of E_1 in equation (38) vanish.

To consider values of $\rho_6, \rho_7, \rho_8, \rho_9$, close to, but not at, the singular value, we consider, for fixed values of ρ_6 and ρ_7, the ellipse: $\rho_8 = \rho_6(1 + r\cos\theta)$ and $\rho_9 = \rho_7(1 + r\sin\theta)$ centred at the singular point $(\rho_8, \rho_9) = (\rho_6, \rho_7)$ and parametrised by $r \geqslant 0$ and $\theta \in [0, 2\pi]$ (see Figure 9(a)). In Figure 9(a) (inset plots), as θ varies we observe four qualitatively different cases. In case (1), the growth rate of R exceeds that of L and we expect steady states with $R \neq 0$; in case (2) L and R dominance exchanges. That is, in a low nutrient (E) environment, L grow at a faster rate than R, however, as the nutrient abundance increases the growth rate of R exceeds that of L. In case (3), the growth rate of L exceeds that of R and we expect steady states with $L \neq 0$, and in (4) L and R dominance exchanges, in a manner similar to that observed for case (2) but with the roles of L and R interchanged.

Figure 9(b) shows how E varies (diagrams for F, L, R are omitted for brevity) as θ varies, with numbers 1 to 4 representing the four cases of L-R dominance as described in Figure 9(a).

In biological terms, since we are interested in healthy CL development (where all four variables are non-zero), a value of $\theta := \theta^s \in (\theta^* = \frac{\pi}{4}, \theta^{**})$ is chosen, which gives a point $S' = (\rho_8^*, \rho_9^*)$ on the ellipse, with $\rho_8^* > \rho_6$, $\rho_9^* > \rho_7$. For these values, the steady state $A_1^s \neq \underline{0}$ exists and is stable. Any case other than (2) implies a pathological CL. In particular, case (1) implies $A_{5a}^s := (0, 0, 0, 1)$, an avascular ($E = 0$) state, where only stromal cells survive ($V = R = 1$). More importantly, there are no LCs, which implies no progesterone production to support embryonic development. Case (3) yields $A_3^s := (F, E, L, 0)$ which may also be regarded as a pathological condition (since $R = 0$), although embryonic development might be sustained due to the presence of LCs. Choosing $\theta := \theta^{ss} = \theta^{s} + \pi \in (\theta^{*'} = \frac{5\pi}{4}, \theta^{**'})$ gives the symmetrical point $\mathrm{S}'' = (\rho_8^{**}, \rho_9^{**})$ with $\rho_8^{**} < \rho_6$, $\rho_9^{**} < \rho_7$, which corresponds to case (4) and the system evolves to either A_{5a}^{s} or A_3^{s}.

Figure 10 shows the bifurcation diagram for the ECs obtained by varying ρ_5 in case (2), corresponding to point S'. The diagram was generated using the expressions for the steady states presented in section 3 and plotting only the segments of the branches which give rise to physically realistic and admissible states (for details, see Appendix B) for all four variables. As ρ_5 varies, different scenarios, with different steady states, arise. For $\rho_5 \in (\rho_5^{*}, \rho_5^{**})$ (intermediate levels of angiogenesis), the system can evolve to the 'healthy' state A_1^{s}. Outside this range, the system evolves to a 'pathogenic' state: $A_3^{s}(R = 0; V = 1)$ for $\rho_5 < \rho_5^{*}$ (weak angiogenesis), or $A_2^{s}(L = 0; V = 1)$, $A_2^{+}(L = 0; V > 1)$, and $A_4^{+}(L = 0, R = 0; V > 1)$ for $\rho_5 > \rho_5^{**}$ (strong angiogenesis).

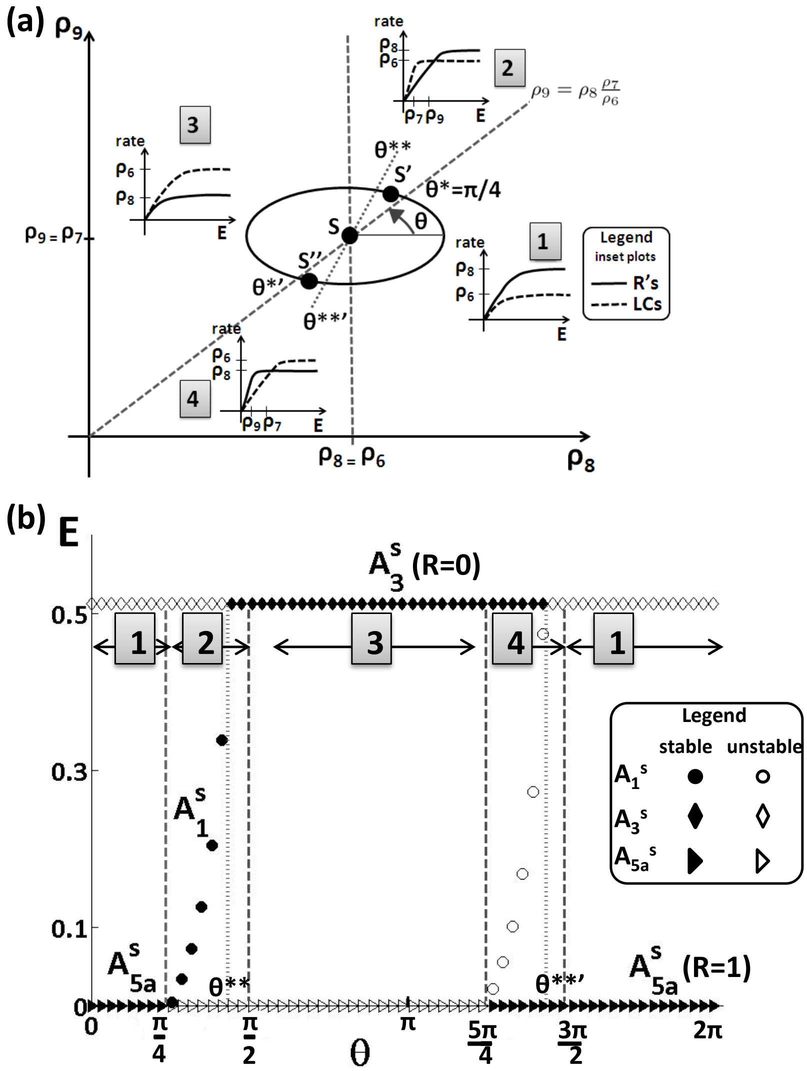

Fig. 9 Steady state CL cellular composition depends on four qualitatively different cases regarding the growth rate of L and R. (a) In the parameter space (ρ_8, ρ_9), we consider the ellipse: $\rho_8 = \rho_6(1 + r\cos\theta)$, $\rho_9 = \rho_7(1 + r\sin\theta)$ (with $r = 0.3$ and $\theta \in [0,2\pi]$) around the singular point $S = (\rho_6, \rho_7)$ at which LCs and stromal cells have the same demand for nutrients and vasculature (E). Inset plots present the four different cases. That is, how the swelling rate of L, given by $\rho_6 \frac{E}{\rho_7+E}$ (dashed curve) as in equation (10), and the proliferation rate of R, given by $\rho_8 \frac{E}{\rho_9+E}$ (solid curve) as in equation (11), change as E varies. (b) Bifurcation diagram showing how the existence and stability of steady state solutions for the ECs vary as the angle θ varies. For conciseness only steady states that are stable for some $\theta \in [0,2\pi]$ are plotted.

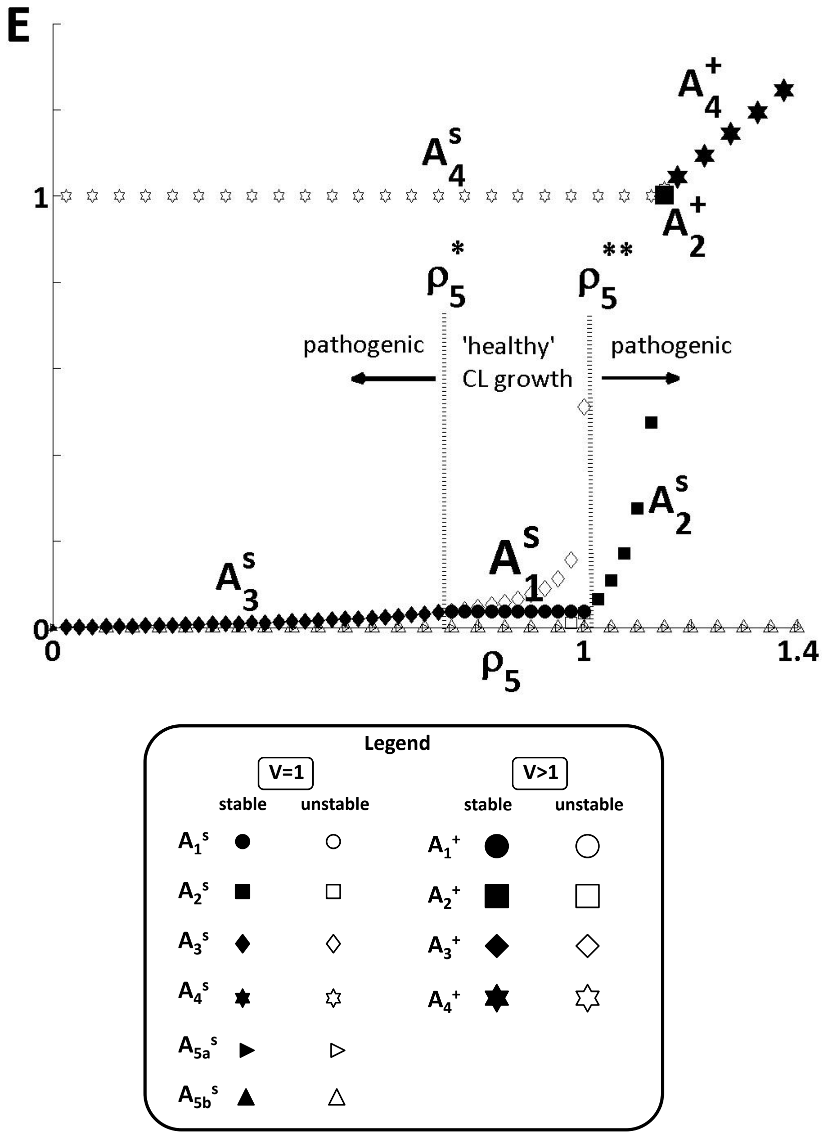

Fig. 10 Bifurcation diagram showing how the existence and stability of steady state solutions for the EC volume (E) vary with ρ_5 (the maximum EC proliferation rate) when $(\rho_8, \rho_9) = (\rho_8^*, \rho_9^*)$ which corresponds to the point S' in Figure 9(a). The steady state solutions are defined in the supporting Legend. Parameter values: as per equation (13) with $\rho_8 = \rho_8^* = 0.81$ and $\rho_9 = \rho_9^* = 0.09$. As ρ_5 varies, three distinct, biologically realistic scenarios are observed: if ρ_5 is too small ($\rho_5 < \rho_5^*$) or too large ($\rho_5 > \rho_5^{**}$), then pathogenic development is predicted because one or more cell types are unable to survive (if $\rho_5 < \rho_5^*$ then $R = 0$; if $\rho_5 > \rho_5^{**}$ then $L = R = 0$). For intermediate values of ρ_5 ($\rho_5^* < \rho_5 < \rho_5^{**}$), healthy CL growth is predicted with $0 < E, L, R$.

4.3 Variation of other parameters

In this section our aim is to check whether the system evolves to a healthy steady state $A_1^{+,s}$ (for which $0 < E, L, R$) by varying parameters for which reliable estimates are not available (see Appendix A). In particular, parameters a_1, a_2 (rates of FGF2 production, by ECs and LCs respectively), and k (a measure of how sensitive the CL cells are to competition for space) were estimated in limiting cases.

For this reason, we use two different cases, labelled (Ia) and (IIa), to estimate a_1 and a_2, and two different cases, (Ib) and (IIb), to estimate k. Briefly, (Ia) represents the limiting case where we assume no LCs (to estimate a_1) and no ECs (to estimate a_2), while (IIa) assumes that FGF2 production from LCs after the first two days of ovulation is minimal (as per Fig 3). (Ib) assumes $F^* \gg F_h$, which implies lower EC proliferation at steady state, while (IIb) assumes $F^* = F_h$. For details see Appendix A. Note that the model studied in section 4.2 uses case (Ia) to estimate a_1, a_2, and (Ib) for k.

The results obtained by combining the above different cases are summarised in Table 4. A combination of (Ia) and (IIb) leads to a change in the steady state from A_1^s to A_1^+. Case (IIb) gives a smaller value for k suggesting that this can lead to a non-constant CL volume (since $V > 1$ at A_1^+). The alternative case for estimating a_1 and a_2 does not seem to lead to a change of the steady state.

Table 4 Table summarising how the estimates of a_1, a_2, k, and the associated stable steady state depend on the cases used for their estimation.

case	a_1	a_2	k	steady state
(Ia) & (Ib)	136	5.1	0.12	A_1^s
(Ia) & (IIb)	136	5.1	0.06	A_1^+
(IIa) & (Ib)	124	0.9	0.12	A_1^s
(IIa) & (IIb)	124	0.9	0.06	A_1^s

An additional parameter which merits further investigation is the decay rate of FGF2, d_F, which has an indirect effect on the EC proliferation rate. Since the decay rate of vascular endothelial growth factor (VEGF), another potent angiogenic factor, has been estimated to be 15 d^{-1} (Owen et al., 2011), which is 5 times larger than the value we use for FGF2, we consider increasing d_F. We recover the steady state A_1^s for a wide range of d_F ($0 < d_F < 15\ d^{-1}$). However, if $d_F > 15\ d^{-1}$, stability shifts from A_1^s to A_4^s. Bifurcations over ρ_5 show bistability between A_3^s and A_4^+ in a certain region of ρ_5. Therefore, depending on the initial conditions, a steady state is feasible either on the discontinuity boundary ($V = 1$) or above it ($V > 1$), where only R (for $A_3^s; V = 1$) or both L and R (for $A_4^+; V > 1$) are zero. By increasing d_F the region of bistability also increases (results not shown due to space limitations).

5 Discussion

In this article, we have developed an ODE model for the growth of the bovine corpus luteum (CL), an organ responsible for progesterone production during pregnancy. Angiogenesis, the process of new blood vessel growth from existing ones, is crucial for CL growth, and inadequate angiogenesis has been linked to infertility in cows. Therefore, by studying the processes which regulate CL development, our aim has been to determine how CL growth is influenced by changes in the parameters associated with endothelial cell proliferation.

The model describes the time evolution of four dependent variables: the concentration of FGF2, and the volume of the endothelial (ECs), luteal (LCs) and stromal cells (R). The ECs represent the vascular density in the CL, while the stromal volume includes cells such as pericytes (PCs). The model is based on the assumption that the CL volume (V) can be approximated by the sum of the volumes of the three cell types, and if V exceeds a threshold value, then cell growth is inhibited. The theoretical surface (Σ) on which the volume threshold is attained is called the *discontinuity boundary.* It separates the model into two different cases (above or below Σ). The resulting model reproduces several features of CL development. That is, a transient surge in FGF2, and CL growth to a steady state volume in which the different cell types are present in proportions that are consistent with experimental observations.

Preliminary insight into the system dynamics was obtained by considering a reduced, two-dimensional model with $L = R = 0$ and $V = E + L + R \approx E$. Given the importance of angiogenesis in the CL, the key bifurcation parameter was taken to be the maximal rate of EC proliferation, ρ_5. If ρ_5 was below a threshold (see equation (16)) the CL volume remained constant ($V = 1$), *sliding* on the discontinuity boundary, and the system evolved to a *pseudo* steady state. Sliding is a special case where trajectories initially either above or below Σ are constrained to lie on Σ. However, if ρ_5 exceeded that threshold, the manifold Σ become unstable and trajectories were attracted to the region $E > 1$ (see Figure 5).

These notable cases observed in the reduced model were the motivation for further investigation into the existence of *pseudo* steady states in the full model. Therefore, in the full model, we analysed the real steady states for the two different vector fields, above and below $\Sigma : E + L + R = 1$, and the *pseudo* steady states, by exploring parameter constraints for which steady states in each region can be physically realistic (non zero) and *admissible* (see definitions in section B).

As for the reduced model, by varying the 'angiogenic parameter', ρ_5, we were able to identify *normal* and *pathological* cases of CL growth (see Figure 10). For low ρ_5, the system evolves to steady state $A_3^s(V = 1)$ characterised by dominance of the LCs and absence of the stromal cells. In this case, although progesterone levels may be high, there are few blood vessels (ECs) to transport progesterone to the uterus. When ρ_5 is high, the CL volume shifts to steady state $A_4^+(V > 1)$ for which the CL is predicted to contain only vessels (ECs), which is biologically implausible. For intermediate values of ρ_5, *healthy* growth of the CL is predicted, and all cellular components are present. This indicates that slight changes in EC proliferation rate (ρ_5) could have a big impact on the CL vasculature, its subsequent growth and function, and thereby, fertility.

Fertility in dairy cows has been continually declining over the past 30 years, with conception rates currently well below 40% (Royal et al., 2000; Lucy, 2001). While the role of ovarian physiology and, in particular, CL growth, development and function have been the main focus of many experimental studies (Lucy, 2001; Mann and Lamming, 2001; Perry et al., 2005; Robinson et al., 2006), mathematical modelling of this biological aspect is scarce. Existing models have focused on hormone production and its regulation during the bovine oestrous cycle (Boer et al., 2011; Pring et al., 2012), while Meier et al. (2009) concentrated on progesterone production. The key hormone, that induces the formation of the CL as well as likely to play an important role in initiating luteal angiogenesis is luteinising hormone (LH) (Robinson et al., 2008). Therefore, it would be interesting in future work to combine our model of CL growth with existing models (1) to investigate influence of LH on CL growth, and (2) to determine how progesterone levels influenced by CL growth. Although our model was motivated from bovine experimental data, the setup of the model is quite generic, and therefore, it could be possible to fit the model to measurement data from human or other species.

We conclude by further discussing possible extensions and improvements to the current model. The results from our model were based on parameter estimates which were chosen as reasonably as possible from independent data. However, future work may involve a more systematic parameter sensitivity analysis to assess the robustness of the results (steady states that the system evolves to). PCs are perivascular cells that are typically associated with ECs in microvessels. Experiments performed by (Redmer et al., 2001) suggest that PCs represent a large proportion of the proliferating cells during the early luteal phase. In the same study, PCs appeared to be among the first cells to migrate into the hypoxic granulosa region after ovulation. It has been suggested that PCs are capable of guiding sprouting processes by migrating ahead of ECs and expressing VEGF, a potent mitogenic factor that can induce the ECs to proliferate subsequent to migration (Redmer et al., 2001). We could extend our model to include multiple angiogenic factors, such as VEGF and FGF2, and also to account for the way in which PCs influence angiogenesis. For example, a CL with low numbers of PCs might be expected to produce a poorly functioning vasculature. The model could also be used to determine whether manipulation of PC levels might restore function to a compromised CL. The ODE model could also be extended to account for spatial effects, either by formulating a continuum model based on PDEs or by using an agent-based model that distinguishes between individual cells.

Acknowledgements SAP acknowledges support from the Schools of Biosciences and Mathematical Sciences at the University of Nottingham in the form of a PhD studentship. MRJ's research is supported by EPSRC grant EP/J001317/1. This publication was based in part on work supported by Award No. KUK-C1-013-04, made by King Abdullah University of Science and Technology (KAUST).

A Estimation of parameter values

Guided by estimates of the maximum proliferation rate of bovine aorta ECs cultured *in vitro*, we suppose initially that the maximum growth rate of all cell types are identical so that $k_E = k_L = k_R \sim 1$ day$(d)^{-1}$ (Lincoln et al., 1982), and later explore the consequences of relaxing this assumption.

Regarding the decay rate of FGF2, we fixed $d_F = 3\ d^{-1}$ since its half-life is ~ 8 hrs (Beenken and Mohammadi, 2009). Concerning F_h, the FGF2 concentration at which the EC proliferation rate is half-maximal, we chose it to be a typical late level of FGF2 ($F*$; see Fig 2(a)), so that $F_h = F* \simeq 50\ ng.(cm^3)^{-1}$. We remark that in Fig 2(a) FGF2 has units ng/g tissue, but since the majority of tissues consist predominantly of water, we convert from ng/g to ng/cm^3 by assuming that 1 g occupies approximately 1 cm^3.

A value of $\overline{V}$ was estimated for the CL volume, above which cells compete for space. From Fig 2(b), the steady value for the CL diameter is approximately 2.5 cm and, therefore, $\overline{V} \simeq \frac{4}{3}\pi R^3 \simeq 8.2\ cm^3$. In mid-cycle, LCs comprise approximately 68% of the bovine CL volume and the ECs approximately 13% (Wiltbank, 1994). Therefore, we assume that E_{h1} and E_{h2}, the volume of ECs at which the swelling rate of LCs and stromal cells is half-maximal, are identical $\sim 13\%\overline{V} = 1.07\ cm^3$.

The above estimates imply that typical proportion of ECs and LCs is ECs:LCs=13:68. Therefore, an estimate for the parameter R_{EL} (as in equation (1)), the value of E/L at which FGF2 production rate (from LCs) is half-maximal was obtained. That is, $R_{EL} = 0.19$.
The methods for estimating the parameters a_1 and a_2, and the parameter k are enumerated below as methods (Ia) and (Ib), respectively.

(Ia). To estimate a_1 and a_2, we assume a steady state $\dot{F}$=0, and solve for a_1 when there are no LCs and solve for a_2 when there are no ECs. Then, for a_1, $\dot{F} = a_1 E - d_F F$, gives $a_1 = d_F \frac{F}{E} \simeq d_F \frac{F*}{E*} \simeq d_F \frac{F*}{0.13\,\overline{V}} \simeq \frac{3*50}{1.1} \simeq 136$. For a_2, $\dot{F} = a_2 \frac{L}{R_{EL}} - d_F F$, gives $a_2 \simeq d_F R_{EL} \frac{F}{L} \simeq d_F R_{EL} \frac{F*}{L*} \simeq d_F R_{EL} \frac{F*}{0.68\,\overline{V}} = \frac{3*0.19*50}{5.6} \simeq 5.1$.

(Ib). To estimate the parameter k, the strength of the tissue constraint to the cell growth or proliferation, we assume a steady state $\dot{E}$=0 by taking the limiting case where FGF2 is sufficiently high ($F* \gg F_h$). Therefore, $\dot{E} = 0 \Rightarrow k_E E = kEV \Rightarrow k = \frac{k_E}{V} \simeq \frac{k_E}{\overline{V}} \simeq 0.12$.

Dimensional estimates of the model parameters in equations (2), (5)-(7) were estimated as accurately as possible. Since there is less data with which to determine a_1, a_2, and k, than the other parameters, we give here an alternative method to estimate them, as a test of robustness. These alternative methods are enumerated below as (IIa) and (IIb):

(IIa). Here we estimate a_1 and a_2 as follows. In Figure 3, a schematic is presented which illustrates the high FGF2 production by LCs during the first two days, while ECs are productive all over the cell cycle. Based on that, we assume that the FGF2 production from LCs after the first two days is minimal. That is, at steady state ($\dot{F} = 0$) $\frac{a_2 L}{R_{EL} + \frac{E}{L}} \to 0$, or equivalently,

$$a_1 E* \gg \frac{a_2 L*}{R_{EL} + \frac{E*}{L*}}. \tag{49}$$

In addition, at steady state,

$$\dot{F} = 0 \Leftrightarrow a_1 E* \left(1 + \frac{1}{\gamma}\right) = d_F F*, \tag{50}$$

where,

$$\gamma = \frac{a_1 E^*}{\frac{a_2 L^*}{R_{EL} + \frac{E^*}{L^*}}} = 0.07 \frac{a_1}{a_2}, \tag{51}$$

is the ratio of FGF2 production by ECs to that by LCs. If $\gamma = 10$, then

$$a_1 \simeq 143\, a_2. \tag{52}$$

Now equation (50) supplies $a_1 = \frac{d_F F^*}{E^*(1+\frac{1}{\gamma})} \simeq 124$, in which case $a_2 \simeq 0.9$.

(IIb). Here we estimate k as follows. We assume a steady state $\dot{E} = 0$ and FGF2 steady value being smaller than for (Ib), e.g. $F^* = F_h$, and solving for k implies: $k \sim \frac{F^*}{F_h + F^*} \frac{k_E}{V} \simeq \frac{1}{2} \frac{k_E}{V} = 0.06$.

B Classification of steady state in Filippov systems

The types of steady states that Filippov systems exhibit are summarised below.

Definition 5.2. A point $\underline{x} \in D$ is termed an *admissible steady state* of (17) if

$$\underline{f}^+(\underline{x}) = 0 \;\; and \;\; \Theta(\underline{x}) > 0, \quad or \;\; \underline{f}^-(\underline{x}) = 0 \;\; and \;\; \Theta(\underline{x}) < 0; \tag{53}$$

a point $\underline{x} \in G^{\pm}$ is termed a *virtual steady state* of (17) if

$$\underline{f}^+(\underline{x}) = 0 \;\; but \;\; \Theta(\underline{x}) < 0, \quad or \;\; \underline{f}^-(\underline{x}) = 0 \;\; but \;\; \Theta(\underline{x}) > 0. \tag{54}$$

Definition 5.3. A point $\underline{x} \in D$ is termed a *pseudo steady state* if

$$\underline{g}(\underline{x}) = 0 \;\; and \;\; \Theta(\underline{x}) = 0. \tag{55}$$

As for Definition 5.2, there may exist solutions to $\underline{g}(\underline{x}) = 0$ which are invalid because $x \in \Sigma \backslash \hat{\Sigma}$. We distinguish such solutions as follows:

Definition 5.4. A *pseudo steady state* is termed *admissible* if $0<\lambda<1$ and *virtual* if $\lambda < 0$ or $\lambda > 1$, with λ as defined in (28).

For some values of the system parameters, a steady state may lie on the discontinuity boundary. Since $\underline{f}^+$ or $\underline{f}^-$ vanishes there, we find that $\underline{g}$ also vanishes by (29), so that a steady state on Σ *always* coincides with a pseudo steady state. Furthermore this occurs on the sliding boundary where $\lambda = 0$ or 1. We classify such points as follows.

Definition 5.5. A point $\underline{x} \in D$ is termed a *boundary steady state* of (17) if

$$\underline{f}^+(\underline{x}) = 0 \;\; and \;\; \Theta(\underline{x}) = 0, \quad or \;\; \underline{f}^-(\underline{x}) = 0 \;\; and \;\; \Theta(\underline{x}) = 0. \tag{56}$$

The admissibility conditions for the steady states in G^+ and $\hat{\Sigma}$ are given below.

Conditions for A_1^+

From equation (38) we deduce that $E_1 \geqslant 0$ if either

$$\frac{\rho_9}{\rho_7} \leqslant \frac{\rho_8}{\rho_6} \leqslant 1 \qquad \text{or} \qquad 1 \leqslant \frac{\rho_8}{\rho_6} \leqslant \frac{\rho_9}{\rho_7}, \tag{57}$$

where $\frac{\rho_8}{\rho_6}$ is the ratio of the maximal growth rate of the stromal cells to that of the luteal cells, and $\frac{\rho_9}{\rho_7}$ is the ratio of the half-maximal EC value of the stromal cells to that of the luteal cells. Similarly, the concentration of $FGF2$, $F = E_1\phi(E_1)$, is physically realistic if $\phi(E_1) \geqslant 0$ where, since $\rho_6 > 0$,

$$\phi(E_1) \geqslant 0 \Leftrightarrow \rho_5\rho_7 + E_1(\rho_5 - \rho_6) \geqslant 0 \Leftrightarrow \frac{\rho_5}{\rho_6} \geqslant \frac{E_1}{\rho_7 + E_1} \Leftrightarrow \rho_5 \geqslant \rho_6 \frac{\frac{\rho_9}{\rho_7} - \frac{\rho_8}{\rho_6}}{\frac{\rho_9}{\rho_7} - 1} \tag{58}$$

since (57) guarantees that $E_1 > 0$. Thus (58) places a lower bound on ρ_5.

The value of L is physically realistic if $\psi(E_1) \geqslant 0$ ($\Leftrightarrow \omega(E_1) \geqslant 0$), which implies

$$\rho_5 \leqslant \frac{\rho_6(\rho_4 + \rho_1 E_1)}{\rho_1(\rho_7 + E_1)}, \tag{59}$$

an upper bound to ρ_5 (since $E_1 \geqslant 0$).

The value of R is physically realistic if $\nu(E_1) - \psi(E_1) \geqslant 1$. Substituting in the expression for ψ (equation (36)) in terms of ω, implies

$$\rho_2\left(\nu(E_1) - 1\right)^2 - \rho_3\omega(E_1)\left(\nu(E_1) - 1\right) \geqslant \omega(E_1) \geqslant 0. \tag{60}$$

The admissibility condition for A_1^+ is simply that the volume $V = V_1^+$ satisfies

$$V_1^+ = E_1\nu(E_1) = \frac{\rho_6\rho_9 - \rho_7\rho_8}{\rho_9 - \rho_7} \geqslant 1. \tag{61}$$

Conditions for A_2^+

The components of A_2^+ are non-negative if

$$E_2 = \frac{\rho_4\rho_8 - \rho_1\rho_5\rho_9}{\rho_1(\rho_5 - \rho_8)} \geqslant 0, \qquad \text{and} \qquad \eta(E_2) = \frac{\rho_8}{\rho_9 + E_2} \geqslant 1. \tag{62}$$

The first inequality supplies the following mutually exclusive set of inequalities:

$$(i)\ 1 \leqslant \frac{\rho_5}{\rho_8} \leqslant \frac{\rho_4}{\rho_1\rho_9},\ \ or\ \ (ii)\ \frac{\rho_4}{\rho_1\rho_9} \leqslant \frac{\rho_5}{\rho_8} \leqslant 1.$$

The second inequality ($\eta(E_2) \geqslant 1$) yields:

$$\rho_5 \geqslant \frac{\rho_4}{\rho_1} + \rho_8 - \rho_9.$$

The admissibility condition for A_2^+ is that the volume $V = V_2^+$ satisfies

$$V_2^+ = E_2\eta(E_2) = \frac{\rho_4\rho_8 - \rho_1\rho_9\rho_5}{\rho_6(\rho_4 - \rho_1\rho_9)} \geqslant 1, \tag{63}$$

noting that $V_2^+ \geqslant 0$ is guaranteed by both cases (i) and (ii) above.

Conditions for A_3^+

The steady state A_3^+ is physically realistic if E_3, $\phi(E_3)$, and $(\nu(E_3) - 1)$ are positive. The solution for E_3 as a root of the cubic polynomial (39) is unilluminating so we do not present it here. We note, however, that (39) has real coefficients, hence it always has at least one real root, but the root may not be positive for all values of the parameters.

The admissibility condition can be written as

$$V_3^+ = E_3\nu(E_3) = \frac{\rho_6 E_3}{\rho_7 + E_3} \geqslant 1. \tag{64}$$

Numerical solutions of these equations for the parameter values in (13), with ρ_5 allowed to vary, reveal only one physically realistic steady state solution, A_3^+. It becomes unphysical outside the left bound as $L = \nu(E_3) - 1$ becomes negative, and inadmissible outside the right bound as $E\Omega = V_3^+ = E_3\nu(E_3)$ becomes smaller than unity.

Conditions for A_4^+

The steady state solution A_4^+ is physically realistic if $E_4 \geqslant 0$, implying $\frac{\rho_5}{\rho_6} - \frac{\rho_4}{\rho_1} \geqslant 0$ or, as a condition on ρ_5,

$$\rho_5 \geqslant \frac{\rho_4}{\rho_1}. \tag{65}$$

The admissibility condition is

$$V_4^+ = \rho_5 - \frac{\rho_4}{\rho_1} \geqslant 1 \quad \Leftrightarrow \quad \rho_5 \geqslant \left(1 + \frac{\rho_4}{\rho_1}\right). \tag{66}$$

Notice that the ratio $\frac{\rho_4}{\rho_1}$ is involved in determining whether both of the steady states A_2^+ and A_4^+ are physically realistic.

We now establish conditions under which the steady states A_n^s are physically realistic and satisfy the conditions for $\hat{\Sigma}$ in Table 2.

Conditions for A_1^s

Because the first three components of A_1^s are the same as A_1^+, the conditions (57)-(59) ensure that E_1, $\phi(E_1)$, and $\psi(E_1)$ are positive. By contrast, the condition for R to be physically realistic becomes $\frac{1}{E_1} - \psi(E_1) - 1 \geqslant 0$. Substituting in the expression for ψ in terms of ω, a little manipulation gives the condition

$$\rho_2 \left(\frac{1}{E_1} - 1\right)^2 - \rho_3\omega(E_1)\left(\frac{1}{E_1} - 1\right) \geqslant \omega(E_1) \geqslant 0. \tag{67}$$

Now consider the admissibility condition $0 \leqslant E\Omega \leqslant 1$. The third ($L$) component of $g(A_1^s)$ from (30), which vanishes because A_1^s is a steady state, gives

$$E_1\Omega = \frac{\rho_6 E_1}{\rho_7 + E_1}.$$

Substituting in E_1 from (38), after a little rearranging the admissibility condition becomes

$$0 \leqslant \frac{\rho_6\rho_9 - \rho_7\rho_8}{\rho_9 - \rho_7} \leqslant 1. \tag{68}$$

Conditions for A_2^s

Physical values of A_2^s require $E_2 \geqslant 0$ and $\frac{1}{E_2} - 1 \geqslant 0$, implying $0 \leqslant E_2 \leqslant 1$, which gives

$$0 \leqslant \frac{\rho_4\rho_8 - \rho_1\rho_5\rho_9}{\rho_1(\rho_5 - \rho_8)} \leqslant 1. \tag{69}$$

As for A_2^+ there are two cases to consider,

(i) $\rho_5 \geqslant \rho_8$ implies $0 \leqslant \rho_4\rho_8 - \rho_1\rho_5\rho_9 \leqslant \rho_1(\rho_5 - \rho_8)$,
(ii) $\rho_5 \leqslant \rho_8$ implies $0 \geqslant \rho_4\rho_8 - \rho_1\rho_5\rho_9 \geqslant \rho_1(\rho_5 - \rho_8)$.

which can be rearranged to give conditions on ρ_5,

(i) $\rho_5 \geqslant \rho_8$ implies $\rho_5 \geqslant \frac{\rho_8}{\rho_1}\frac{\rho_1+\rho_4}{1+\rho_9}$ and $\rho_5 \leqslant \frac{\rho_4\rho_8}{\rho_1\rho_9}$,
(ii) $\rho_5 \leqslant \rho_8$ implies $\rho_5 \leqslant \frac{\rho_8}{\rho_1}\frac{\rho_1+\rho_4}{1+\rho_9}$ and $\rho_5 \geqslant \frac{\rho_4\rho_8}{\rho_1\rho_9}$.

To evaluate the admissibility condition on $E\Omega$, consider the fourth (R) component of $g(A_2^s)$ from (30), which vanishes because A_1^s is a steady state, and therefore gives

$$E_2\Omega = \frac{\rho_8 E_2}{\rho_9 + E_2}.$$

Substituting in E_2 from (38) and rearranging gives $E_2\Omega = \frac{\rho_4\rho_8 - \rho_1\rho_5\rho_9}{\rho_4 - \rho_1\rho_9}$, hence the admissibility condition becomes

$$0 \leqslant \frac{\rho_4\rho_8 - \rho_1\rho_5\rho_9}{\rho_4 - \rho_1\rho_9} \leqslant 1. \tag{70}$$

Equation (70) consists of two cases:

(a) $\rho_4 < \rho_1\rho_9$ implies $\rho_5 \geqslant \frac{\rho_4\rho_8}{\rho_1\rho_9} - \frac{\rho_4}{\rho_1\rho_9} + 1$,
(b) $\rho_4 > \rho_1\rho_9$ implies $\frac{\rho_4\rho_8}{\rho_1\rho_9} - \frac{\rho_4}{\rho_1\rho_9} + 1 \leqslant \rho_5 < \frac{\rho_4\rho_8}{\rho_1\rho_9}$, and this can only happen in case (i).

Conditions for A_3^s

For the state A_3^s to be physically realistic requires that the three quantities E_3^s, $\phi(E_3^s)$, and $\frac{1}{E_3^s} - 1$, are positive. As for A_3^+, the cubic root solution for E_3^s is unilluminating, but we note that (44) always has at least one real root which need not be positive for all values of the parameters.

The third (L) component of $g(A_3^s)$ from (30), which vanishes because A_3^s is a steady state, gives

$$E_3^s\Omega = \frac{\rho_6 E_3^s}{\rho_7 + E_3^s},$$

with which the admissibility condition can be written as

$$0 \leqslant \frac{\rho_6 E_3^s}{\rho_7 + E_3^s} \leqslant 1, \tag{71}$$

in terms of the cubic root E_3^s.

Conditions for A_4^s

The condition for A_4^s to be physically realistic is simply $E_4 > 0$, which gives (65). For the admissibility condition, note that using the second (E) component of $g(A_4^s)$, which vanishes since A_4^s is a steady state, we can write $E_4\Omega = \frac{\rho_5 F}{1+F} = \frac{\rho_1\rho_5}{\rho_1+\rho_4}$, and therefore admissibility requires $0 \leqslant \frac{\rho_1\rho_5}{\rho_1+\rho_4} \leqslant 1$, which rearranges to

$$0 \leqslant \rho_5 \leqslant 1 + \frac{\rho_4}{\rho_1}. \tag{72}$$

C Stability of the plane Π^-

The stability of the plane Π^- (as defined in equation (46) is of some importance being a distributed object in the regions G^- and $\hat{\Sigma}$. It is also rather more simple to express, requiring the calculation of stability in only two directions orthogonal to each other and to the plane.

To determine whether Π^- is an attractor we first take coordinates $u_1 = E$, $u_2 = F - \rho^* L$, $u_3 = \rho^* F + L$, $u_4 = R$, where $\rho^* = \frac{\rho_2}{\rho_3\rho_4}$. The u_i form an orthogonal coordinate system, since $\nabla u_i \cdot \nabla u_j = 0$ for all $i \neq j \in (1,2,3,4)$ with $\nabla = \left(\frac{d}{dF}, \frac{d}{dE}, \frac{d}{dL}, \frac{d}{dR}\right)$. The u_1 and u_2 coordinate axes lie perpendicular to Π^- (so Π^- is the plane $u_1 = u_2 = 0$), while u_3 and u_4 form a coordinate system over the plane Π^-.

The Jacobian of the u_1, u_2 system at $u_1 = u_2 = 0$ expresses the derivative of the flow through Π^-. Using $\dot{u}_1 = \dot{E}$ and $\dot{u}_2 = \dot{F} - \rho^* \dot{L}$, this is given by

$$J_{\Pi^-} = \begin{pmatrix} \frac{\partial \dot{u}_1}{\partial u_1} & \frac{\partial \dot{u}_1}{\partial u_2} \\ \frac{\partial \dot{u}_2}{\partial u_1} & \frac{\partial \dot{u}_2}{\partial u_2} \end{pmatrix}_{|u_1=u_2=0} = \begin{pmatrix} \frac{\rho_5 u_3 \rho^*}{u_3\rho^* + \sqrt{1+\rho^{*2}}} & 0 \\ \rho_1 - \rho^* \frac{\rho_4}{\rho_3} - \frac{\rho_7 \rho^* u_3}{\rho_8 \sqrt{1+\rho^{*2}}} & -\rho_4 \frac{1+3\rho^{*2}}{\sqrt{1+\rho^{*2}}} \end{pmatrix},$$

with eigenvalues $\mu_1 = -\rho_4 \frac{1+3\rho^{*2}}{\sqrt{1+\rho^{*2}}}$ and $\mu_2 = \frac{\rho_5 u_3 \rho^*}{u_3\rho^* + \sqrt{1+\rho^{*2}}}$. Note that $\mu_1 < 0$ since $\rho^* > 0$. Also $u_3 = \rho^* F + L > 0$ given that $F, L > 0$, and therefore $\mu_2 > 0$.

As a result, the plane Π^- is of *'saddle type'*, having one stable and one (orthogonal) unstable direction. Π^- is therefore not a global attractor.

References

Beenken, A. and M. Mohammadi (2009). The FGF family: biology, pathophysiology and therapy. *Nat Rev 8*, 235–253.

Bernardo, M., C. Budd, A. Champneys, and P. Kowalczyk (2008). Piecewise-smooth dynamical systems: theory and applications. *Springer*.

Boer, H., C. Stotzel, S. Roblitz, P. Deuflhard, R. Veerkamp, and H. Woelders (2011). A simple mathematical model of the bovine estrous cycle: Follicle development and endocrine interactions. *J Theor Biol 278*, 20–31.

Colombo, A. (2009). A bifurcation analysis of discontinuous systems: theory and applications. *Dissertation, Politecnico di Milano, Italy*.

Filippov, A. (1982). Differential equations with discontinuous righthand sides. *Kluwer Academic Publishers, Dordrecht, The Netherlands 56*, 281–292.

Fraser, H. and S. Lunn (2001). Regularization and manipulation of angiogenesis in the primate corpus luteum. *Reprod 121*, 355–362.

Hunter, R. (2003). Physiology of the graafian follicle and ovulation. *Cambridge University press*.

Juengel, J. and G. Niswender (1999). Molecular regulation of luteal progesterone synthesis in domestic ruminants. *J Reprod Fert Supp 54*, 193–205.

Kuznetsov, Y., S. Rinaldi, and A. Gragnani (2003). One-parameter bifurcations in planar filippov systems. *IJBC 13*, 2157–2188.

Laird, M. (2010). Angiogenesis during luteal development in the cow. *Dissertation, University of Nottingham, UK*.

Laird, M., K. Woad, M. Hunter, G. Mann, and R. Robinson (2013). Fibroblast growth factor 2 induces the precocious development of endothelial cell networks in bovine luteinising follicular cells. *Reprod Fertil Dev 25*, 372–386.

Lincoln, D., R. Whitney, and J. Smith (1982). In vitro proliferation and lifespan of bovine aorta endothelial cells: response to conditioned media. *J Cell Sci 56*, 281–292.

Lucy, M. (2001). Reproductive loss in high-producing dairy cattle: Where will it end? *J Dairy Sci 84*, 1277–1293.

Mann, G. (2009). Corpus luteum size and plasma progesterone concentration in cows. *Anim Reprod Sci 115*, 296–299.

Mann, G. and G. Lamming (2001). Relationship between maternal endocrine environment, early embryo development and inhibition of the luteolytic mechanism in cows. *Reprod 121*, 175–180.

Meier, S., J. Roche, E. Kolver, and R. Boston (2009). A compartmental model describing changes in progesterone concentrations during the oestrous cycle. *J Dairy Res 76*, 249–256.

Owen, R., I. Stamper, M. Muthana, G. Richardson, J. Dobson, C. Lewis, and H. Byrne (2011). Mathematical modeling predicts synergistic antitumor effects of combining a macrophage-based, hypoxia-targeted gene therapy with chemotherapy. *Cancer Res 71*, 2826–2837.

Perry, G., M. Smith, M. Lucy, J. Green, T. Parks, M. MacNeil, A. Roberts, and T. Geary (2005). Relationship between follicle size at insemination and pregnancy success. *PNAS 102*, 5268–5273.

Piiroinen, P. and Y. Kuznetsov (2008). An event-driven method to simulate filippov systems with accurate computing of sliding motions. *ACM Trans. Math. Softw. 34*(3).

Pring, S., M. Owen, J. King, K. Sinclair, R. Webb, A. Flint, and P. Garnsworthy (2012). A mathematical model of the bovine oestrous cycle: Simulating outcomes of dietary and pharmacological interventions. *J Theor Biol 313*, 115–126.

Redmer, D., V. Doraiswamy, B. Bortnem, K. Fisher, A. Jablonka-Shariff, A. Grazul-Bilska, and L. Reynolds (2001). Evidence for a role of capillary pericytes in vascular growth of the developing ovine corpus luteum. *Biol Reprod 65*(3), 879–889.

Reynolds, L. and D. Redmer (1996). Angiogenesis in the ovary. *Rev Reprod 1*, 182–192.

Reynolds, L. and D. Redmer (1998). Expression of the angiogenic factors, bFGF and VEGF, in the ovary. *J Anim Sci 76*, 1671–1681.

Reynolds, L. and D. Redmer (1999). Growth and development of the corpus luteum. *J Reprod Fert Supp 54*, 181–191.

Rieck, P., L. Oliver, K. Engelmann, G. Fuhrmann, C. Hartmann, and Y. Courtois (1995). The role of exogenous/endogenous basic fibroblast growth factor (FGF2) and transforming growth factor β (TGFβ-1) on human corneal endothelial cells proliferation in vitro. *Exp Cell Res 220*, 36–46.

Robinson, R., A. Hammond, M. Hunter, and G. Mann (2008). A novel physiological culture system that mimics luteal angiogenesis. *Reprod 9*, 433–457.

Robinson, R., A. Hammond, L. Nicklin, D. Schams, G. Mann, and M. Hunter (2006). Endocrine and cellular characteristics of corpora lutea from cows with a delayed post-ovulatory progesterone rise. *Dom Anim Endo 31*, 154–172.

Robinson, R., L. Nicklin, A. Hammond, D. Schams, M. Hunter, and G. Mann (2007). Fibroblast growth factor 2 is more dynamic than vascular endothelial growth factor A during the follicle-luteal transition in the cow. *Biol Reprod 77*, 28–36.

Robinson, R., K. Woad, A. Hammond, M. Laird, M. Hunter, and G. Mann (2009). Angiogenesis and vascular function in the ovary. *Reprod 138*, 869–881.

Royal, M., G. Mann, and A. Flint (2000). Strategies for reversing the trend towards subfertility in dairy cattle. *Vet J 160*, 53–60.

Schams, D., B. Berisha, M. Steffl, and W. Amselgruber (2006). Changes in FGF2 and its receptors in bovine follicles before and after GnRH application and after ovulation. *Reprod 131*, 319–329.

Wiltbank, M. (1994). Cell types and hormonal mechanisms associated with mid-cycle corpus luteum function. *J Anim Sci 72*, 1873–1883.